AMPLITUDE MODULATION IN TURBULENT BOUNDARY LAYER OVER ANISOTROPIC PERMEABLE WALL

Xiaonan Chen, Zhixiang Feng, Qingqing Ye
State Key Laboratory of Fluid Power and Mechatronic Systems, Department of Mechanics
Zhejiang University
Hangzhou 310027, China
qingqing_ye@zju.edu.cn

ABSTRACT

In this study, the amplitude modulation effect in a turbulent boundary layer over anisotropic permeable wall was investigated experimentally. The streamwise and wall-normal velocity fields were measured using time-resolved particle image velocimetry. Over the porous surface, the positive and negative large-scale velocity streaks produce suppression and enhancement effects to the near-wall small-scale turbulence, respectively, which is contrary to the conventional effect over the smooth surface. To clarify the coherent structures related to the amplitude modulation effect over the porous surface, large-scale structures were extracted from a low-pass filtered streamwise fluctuation velocity distribution, which is remarkable suppressed by the permeable surface. The amplitude modulation indicates a much weaker correlation between outer large-scale structure and near-wall small-scale turbulence. Overall skin friction reduction was obtained over permeable wall.

INTRODUCTION

Porous media widely exists in nature and engineering applications. Research over the past few decades indicates that the porous wall enhances the intensity of momentum exchange around the porous interface, affecting the turbulent intensity and skin friction (Breugem et al., 2006). Over the porous wall, the fluid flow penetrates the wall due to a weakening of the wall-blocking effect. Breugem et al. (2006) observed the transport of momentum by upwelling and downwelling motion using direct numerical simulation (DNS). The momentum exchange leads to the growth of Kelvin–Helmholtz (K-H) instability and the possible formation of spanwise rollers. For the isotropic porous media, the skin friction increases monotonically with the increase in permeability. However, the distribution and intensity of turbulent coherent structures could be manipulated by the anisotropic porous media(Kuwata and Suga, 2017). By performing DNS, Gómez-de Segura and García-Mayoral (2019) found that the spanwise K-H rollers only appear over anisotropic porous wall with high wall-normal permeability, revealing the strong impact of the porous interior structure. The slip velocity obtained at the porous interface is reported to lead to the skin friction reduction (Feng and Ye, 2023)

Recent works focus on the interaction between large-scale structure and small-scale turbulence, known as amplitude modulation (AM) (Hutchins and Marusic, 2007). Efstathiou and Luhar (2018) gave the first indirect evidence of the amplitude modulation phenomenon over the permeable wall. They found that the skewness of the near-wall velocity measurements is positive with a magnitude larger than that of the smooth-wall case. This result suggests that the correlation coefficient between the large-scale fluctuations and the large-scale envelope of small-scale fluctuation is positive. The AM phenomenon in permeable-wall turbulence was further proven and quantified by Kim et al. (2020). They found that the AM effect was enhanced on the permeable porous wall as compared to the impermeable smooth-wall flow case, indicating the enhanced coherence of the large-scale structures.

Unlike the work of (Kim et al., 2020), which elucidated the amplitude modulation phenomenon in a turbulent boundary layer over a permeable wall which results in increased skin friction, the structured porous media employed in the current study demonstrated potential for reducing drag and noise in a turbulent boundary layer (Feng and Ye, 2023). The present study aims to quantitatively investigate the amplitude modulation phenomenon of large-scale structures on small-scale turbulence and clarify the coherent structures related to this phenomenon in the turbulent boundary layer over a structured porous wall. Structured porous media with uniformly distributed circular pores was applied on a flat plate. Time-resolved planar PIV is applied to capture the instantaneous flow field. The large-scale motions and the small-scale energetic events were extracted. The relation between large- and small- scale structures is analyzed by the amplitude modulation coefficient.

EXPERIMENTAL SETUP

The experiment was performed in a closed-loop type wind tunnel at the Institute of Fluid Engineering of Zhejiang University with a test section of 1,500 mm, a width of 500 mm, and a height of 400 mm, as shown in Fig.1 (a). The freestream velocity was set at approximately 10.5 m/s. The turbulent intensity was controlled below 0.5%. The turbulent boundary layer was developed over a flat aluminum plate of 630 mm in length, 400 mm in width, and 20 mm in thickness. The leading edge of the flat plate is modified into a super-elliptical shape to inhibit the flow separation. A 10 mm width tripping device was installed at 100 mm downstream from the leading edge to promote boundary layer transition. The porous insert of 50 mm in length, 100 mm in width, and 20 mm in thickness was embedded in the plate, as shown in Fig.1 (a). The upstream edge of the porous wall is 278 mm downstream of the leading edge of the boundary layer trip, establishing fully turbulent conditions before reaching the porous section in the present study.

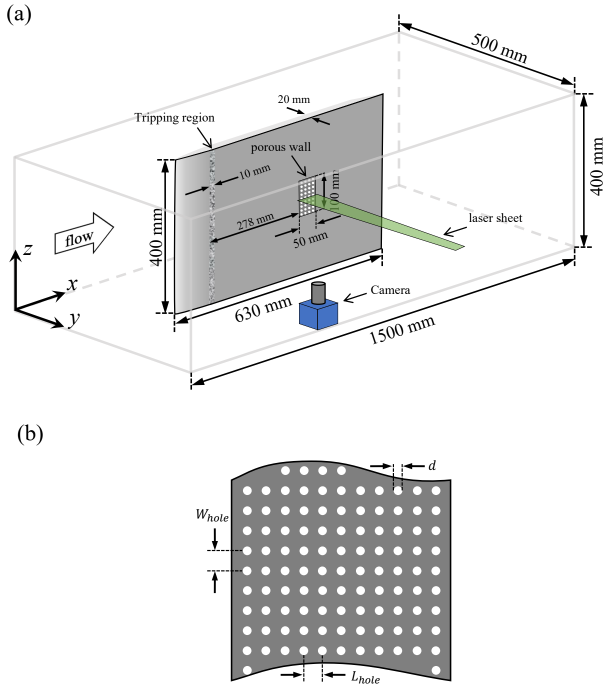

Figure 1. The schematics of: (a) the test section; (b) the porous media.

Two kinds of 3D-printed porous media were used to test the effect of pore size on the coherent structures in the turbulent boundary layer. For both cases, cylindrical channels are evenly distributed over the porous surface, as shown in Fig.1 (b). Two different hole diameters and porosity were applied. For the first configuration, the diameter of the hole is $d_{hole} = 1$ mm (referred to as “small hole”). The streamwise and spanwise distance between the centre of two adjacent holes is $L_{hole} = 1.5$ mm and $W_{hole} = 1.6$ mm, respectively. The second configuration has a hole diameter of $d_{hole} = 2$ mm (referred to as “big hole”). The streamwise distance is $L_{hole} = 4.2$ mm, and the spanwise distance is $W_{hole} = 4.6$ mm. The porosity σ is approximately 32.7% and 16.3% for the small and the big hole cases, respectively.

The planar particle image velocimetry (PIV) technique was used to measure the streamwise and wall-normal velocity field in the $x-y$ plane. As shown in Fig.1 (a), the high-speed camera (Photron FASTCAM Mini AX100, 1024×1024 pixels) equipped with an objective of 105 mm focal length was arranged at the bottom of the test section. The measurement domain of 50×20 mm ($x \times y$) started from 5 mm upstream of the porous section was illuminated by a high-speed laser (Nd: YLF, 527 nm, 50 mJ/pulse at 1 kHz). The resultant digital image resolution is 20 pixels mm^{-1}. The sampling frequency was set as 2 kHz. The ensemble size of the dataset is 4000 (about 2 s). The 2D velocity field was evaluated by a multi-pass cross-correlation method with window deformation. The final interrogation window size is 12×12 pixels with an overlap of 75%, resulting in a vector pitch of 0.15 mm.

1 GLOBAL FLOW CHARACTERIZATION

The profiles of boundary layer properties for the smooth and porous wall cases are shown in Fig.2. The global representation of the quantities is provided by the double-average of the flow field (with the notation $\langle\bar{\cdot}\rangle$). For both smooth and porous wall boundary layers, a clear logarithmic region is observed. As a result, the friction velocity u_τ is estimated by fitting the mean velocity distribution with the Musker profile(Musker, 1979; Kendall and Koochesfahani, 2008) and modified Clauser chart method (Perry and Li, 1990) for smooth and porous wall cases, respectively. As shown in Fig.2 (a), the streamwise mean velocity profile of the smooth wall case fits well with the logarithmic equation of the turbulent boundary layer. For the porous wall cases, the logarithmic region in the mean velocity profiles is denoted by the dash black line and is given by(Mejia-Alvarez, 2010):

$$U^+ = \frac{1}{\kappa} ln(y+d)^+ + B - \Delta U^+ \tag{1}$$

where $\kappa = 0.38$ and $B = 5.4$, d is the zero-plane displacement. Compared with the smooth wall case, the mean velocity profiles for both the porous wall cases show an upward shift, suggesting a decreased wall shear stress. Such decrease in flow resistance results from the relaxation of the no-slip condition caused by the wall permeability (Breugem et al., 2006). The skin friction is also estimated, indicating a reduction of 20.8% and 23.5% for small and big hole cases, respectively. The result in the current research is different from the case over rough surfaces and porous walls with high permeability. In these researches, the growth of strong spanwise coherent structures contributes to the increase of shear stress close to the wall. The details of the boundary layer properties are summarized in TABLE 1.

For the turbulent statistics, a reduction in the R.M.S. of the streamwise velocity fluctuations ($\langle\overline{u^2}\rangle/U_\infty$) and Reynolds shear stress ($\langle-\overline{uv}\rangle/U_\infty^2$) is obtained in the range of $(y+d)/\delta \leq 0.4$, as shown in Fig.2 (b) and (d), which is consistent with the change in friction velocity. Further away from the wall in the outer layer ($(y+d)/\delta > 0.4$), both $\langle\overline{u^2}\rangle/U_\infty$ and $\langle-\overline{uv}\rangle/U_\infty^2$ collapse with that of smooth wall condition. For the R.M.S. of wall-normal velocity fluctuations ($\langle\overline{v^2}\rangle/U_\infty$), although the wall-blocking effect is weakened due to permeability, the magnitude increases near the wall ($(y+d)/\delta \leq 0.1$) due to the upwash and downwash motions. The big hole introduces stronger fluid exchange across the porous interface, which contributes to a higher level of $\langle\overline{v^2}\rangle/U_\infty$ compared with the small hole case. In the range of $0.2 \leq (y+d)/\delta \leq 0.4$, the intensity of wall-normal velocity fluctuations decreases over the porous wall, reaching a lower level compared with the smooth wall condition and indicating a reduced number of turbulent activity in the former range. The characteristics of the turbulent boundary layer over the smooth and porous wall are calculated, as summarized in TABLE 1.

2 LARGE-SCALE STRUCTURES

The momentum transport across the porous interface influences the distribution and strength of large-scale coherent structures(Breugem et al., 2006; Kim et al., 2020; Feng and Ye, 2023). In this section, the effect of the porous walls on the characteristics of large-scale structures is quantitatively investigated. The snapshots of the Gaussian-filtered distribution of streamwise velocity fluctuations are shown in Fig.3. The extracted large-scale structures in the $x-y$ plane for three different cases are shown by the dash black lines. In all cases, the large-scale structures are dominated by the alternative high- and low-speed streaks in the streamwise direction. The mo-

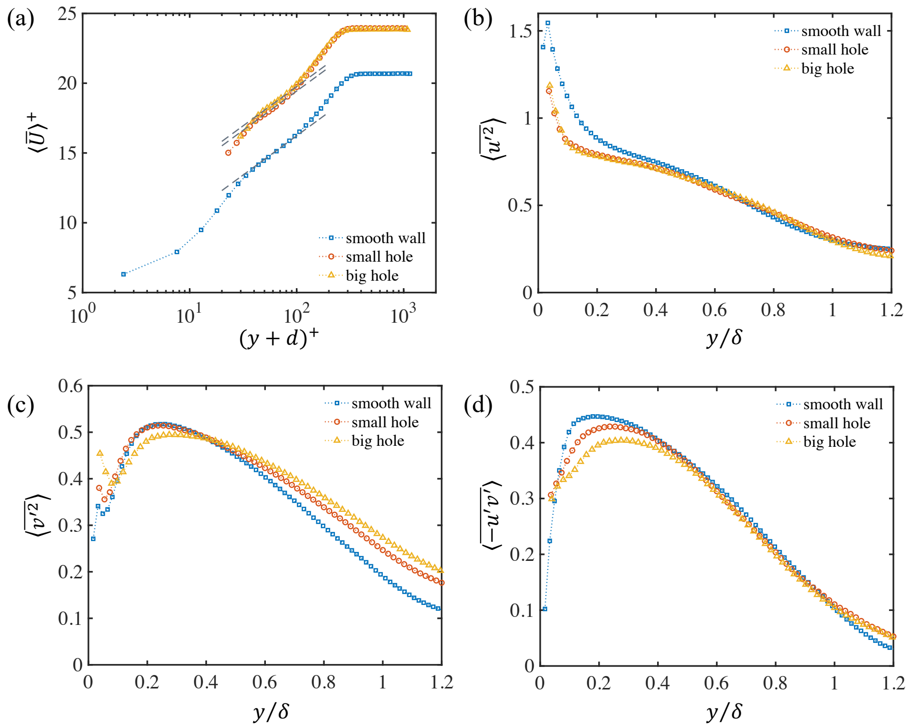

Figure 2. Wall-normal profiles of boundary layer properties: (a) streamwise velocity ($\langle\overline{U}\rangle^+$) (b) R.M.S. of the streamwise velocity fluctuations ($\langle\overline{u^2}\rangle/U_\infty$) ; (c) R.M.S. of the wall-normal velocity fluctuations ($\langle\overline{v^2}\rangle/U_\infty$) ; (d) Reynolds shear stress ($\langle-\overline{uv}\rangle/U_\infty^2$).

Wall model	U_∞ (m/s)	δ (mm)	θ (mm)	u_τ (m/s)	σ	$K(\mathrm{m}^2)$	Re_τ	Re_θ	Re_K
smooth wall	10.5	9.3	1.1	0.510	-	-	319	783	-
small hole	10.7	8.3	0.90	0.446	33.7%	8.3×10^{-9}	250	649	1.59
big hole	10.8	7.7	0.78	0.454	16.3%	1.6×10^{-8}	236	571	2.24

Table 1. Boundary layer properties over smooth and porous wall.

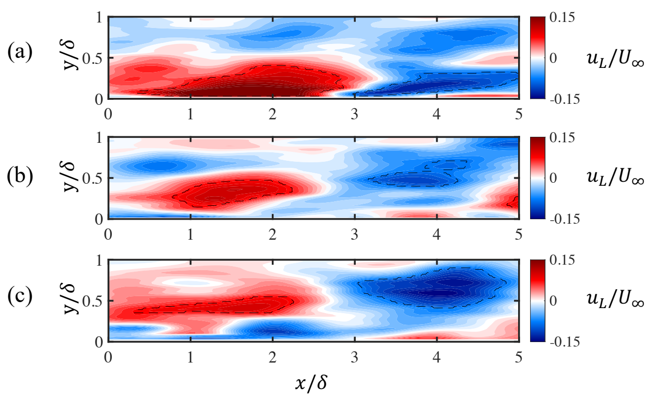

Figure 3. Large-scale structures shown by the $x-y$ cross-plane contour of instantaneous streamwise velocity fluctuations, (a) smooth wall; (b) small hole; (c) big hole. Dash black contour line: extracted large-scale structures.

mentum transport leads to the decrease of the streamwise length of the velocity steaks as shown in Fig.3(b)(c), indicating the disruption of large-scale structures.

The population of the large-scale structures is quantitatively analyzed by the ratio between the time-averaged length of the extracted large-scale structures and the length of the measurement domain $\overline{L_{LSMs}}/L_{domain}$ at each wall-normal height, as shown in Fig.4. The $\overline{L_{LSMs}}/L_{domain}$ undergoes a magnitude decrease with the increase of the wall-normal position for all cases. In the range of $y/\delta < 0.3$, $\overline{L_{LSMs}}/L_{domain}$ for both porous wall cases is remarkably smaller than that of the smooth wall case. The results further quantitatively confirm that the porous wall has a significant disruption effect on the large-scale structures in the near-wall region, to which the reduction of streamwise velocity fluctuations and Reynolds shear stress are related (Ganapathisubramani et al., 2003). The lowest number of large-scale structures appears for the big hole case, whose permeability is higher than the small hole case. Consequently, the effect of the porous wall on the large-scale structure depends on permeability, which directly determines the intensity of wall-normal motions. The upwash and downwash motions induce the growth of K-H instability (Breugem et al., 2006; Manes et al., 2011). However, as discussed by Feng and Ye (2023), no spanwise rollers appear in the instantaneous flow field, indicating that the disturbance energy induced by the K-H instability remains at a relatively low level. The result agrees with those that obtain a skin friction reduction effect (Kuwata and Suga, 2017). In the region away from the wall ($y/\delta > 0.3$), the curves for negative large-scale

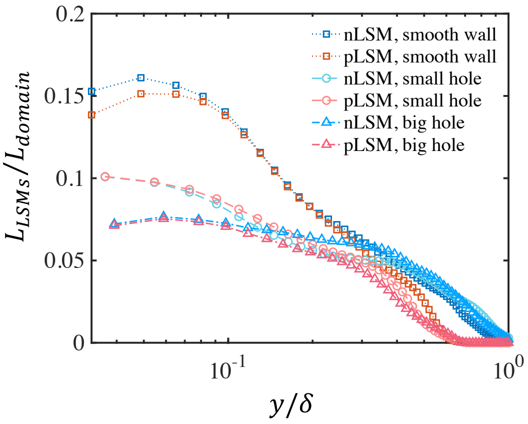

Figure 4. The ratio between the time-averaged length of the extracted large-scale structures and the length of the measurement domain ($\overline{L_{LSMs}}/L_{domain}$) at different wall-normal locations.

structures collapse for all cases. Whereas for positive structure, the number of occurrences over the porous wall remains lower than that of the smooth wall case, suggesting a stronger suppression effect.

3 SMALL-SCALE TURBULENCE

The near-wall small-scale turbulence is the direct contributor to the skin friction(Ganapathisubramani et al., 2003). Over the porous wall, the formation of large-scale low- and high-momentum structures influences the relative intensity of sweep and ejection motions close to the porous interface (Manes et al., 2011; Feng and Ye, 2023). The effect of the porous wall on the small-scale turbulence is characterized by conditional averaged streamwise and wall-normal velocity fluctuations distribution when the VISA events are detected at near wall region ($y/\delta = 0.05$), as shown in Fig. 5 For the smooth wall case at $y/\delta = 0.05$, as shown in Fig. 5 (a,d), the detected VISA events are mainly caused by the sweep (Q4, $u' > 0$ and $v' < 0$) and ejection (Q2, $u' < 0$ and $v' > 0$) events(Blackwelder and Kaplan, 1976). The intensity of the sweep motion is slightly higher than the ejection motion (Wallace et al., 1972; Suga et al., 2011; Feng and Ye, 2023). The streamwise extent of the high-speed region related to the detected VISA events reaches almost 2δ, with the topmost point extending up to $y/\delta = 0.4$. These results suggest that the detected small-scale turbulence is highly related to the large-scale components in the turbulent boundary layer(Chen et al., 2021). Differently, for the porous wall cases (i.e., Fig. 5 (b,e) and (c,f) for small and big holes, respectively), the detected VISA events are mainly induced by the upwash motion ($u' < 0$ and $v' > 0$), transporting low-speed fluid away from the wall. The stronger upwash motion induced over the big hole case contributes to the intensification of small-scale turbulence compared with the small hole case. On the other hand, the sweep events become negligible over both porous wall conditions, indicating a notable suppression. Compared to the smooth wall case, the streamwise and wall-normal extent of the low-speed region for the porous wall case reduces significantly. It has been found that over the smooth wall condition, the positive large-scale motion excites the growth of small-scale turbulence close to the wall (Chung and McKEON, 2010; Hutchins et al., 2011; Pathikonda and Christensen, 2019). Consequently, the disruption of positive large-scale motions (see Fig. 4) causes the possible suppresses small-scale sweep motions in the near-wall region.

4 AMPLITUDE MODULATION

To quantitatively investigate the interaction between the large-scale motions on the small-scale fluctuations over the porous wall, the amplitude modulation effect is analyzed. The amplitude modulation coefficient is defined as the correlation coefficient between the large-scale velocity fluctuations and the low-passed filtered envelope of the small-scale velocity fluctuations (Mathis et al., 2009; Liu et al., 2019). In current study, the streamwise velocity fluctuations are spatially decomposed into large-scale u_L and small-scale u_S components using Gaussian filter in the streamwise direction(Hwang et al., 2016). The two-point correlation $R_u(y1, y2)$ between the large-scale streamwise velocity fluctuations $u_L(y1)$ and the large-scale filtered envelope of the small-scale streamwise velocity fluctuations $E_L(u_S(y2))$ is calculated following Mathis et al. (2009), as:

$$R_u(y1,y2) = \frac{\langle \overline{u_L(y1)E_L(u_S(y2))} \rangle}{\sqrt{\langle \overline{u_L^2(y1)} \rangle}\sqrt{\langle \overline{E_L^2(u_S(y2))} \rangle}} \tag{2}$$

Here, $y1$ and $y2$ represent the wall-normal position where the large-scale and small-scale components are captured, respectively. The notation $\langle \cdot \rangle$ represents the spatial averaging(Wu et al., 2019).

The contour maps of the amplitude modulation coefficient for the porous and smooth walls are shown in Fig.6. For the smooth wall case (Fig.6 (a)), the imprint of the outer large-scale structures modulating the near wall small-scale motions is identified by the strong off-diagonal negative and positive correlation peaks for $y1 < y2$ and $y1 > y2$, respectively (Bernardini and Pirozzoli, 2011). This result is consistent with previous studies over smooth wall turbulent boundary layer(Pathikonda and Christensen, 2019; Kim et al., 2020). The positive amplitude modulation coefficient for $y1 < y2$ is linked to increasing VISA events under positive large-scale structures and decreasing VISA events under negative large-scale motions(Chen et al., 2021). The negative amplitude modulation coefficient for $y1 > y2$ is explained as that the small-scale collision between Q2 and Q4 events caused by hairpin vortex tends to exist on the negative large-scale motions(Adrian, 2007; Elsinga et al., 2010; Dennis and Nickels, 2011). However, for both porous wall cases, the positively correlated region for $y1 > y2$ completely disappears, turning into a weak negative region. The magnitude of the negative correlation coefficient for $y1 < y2$ also decreases, suggesting a weakened inner-outer interaction. Consequently, the upwash and downwash motions over the porous wall lead to a much weaker modulating effect on the small-scale turbulence (Feng and Ye, 2023), contributing to skin friction reduction. Moreover, comparing Fig.6 (b) and (c), it is revealed that porous wall with big holes has a more significant decreasing effect on the magnitude of amplitude modulation coefficient than the case of the small hole. The amplitude modulation effect over the anisotropic porous wall is different from the observation of Kim et al. (2020) over isotropic porous wall case, since they found an enhanced coherence of large-scale spanwise structures, leading to skin friction increase.

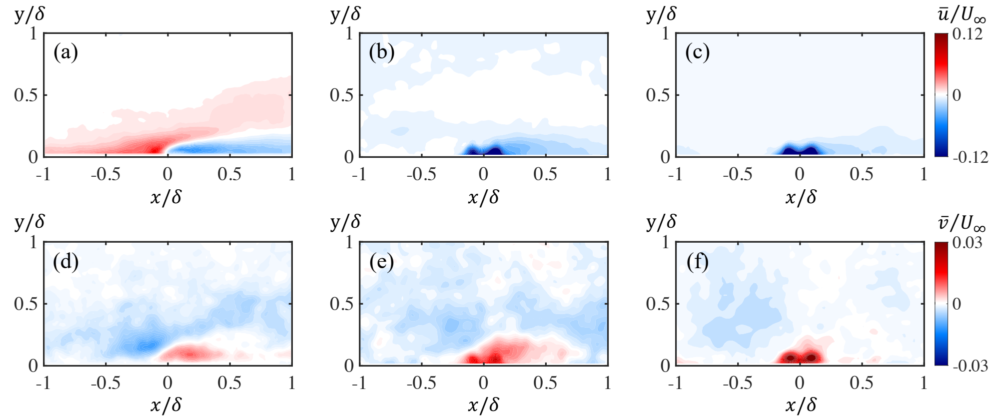

Figure 5. Conditional averaged streamwise and wall-normal velocity fluctuation distribution when small-scale VISA events are detected at $y/\delta = 0.05$: (a,d) smooth wall; (b,e) small hole; (c,f) big hole.

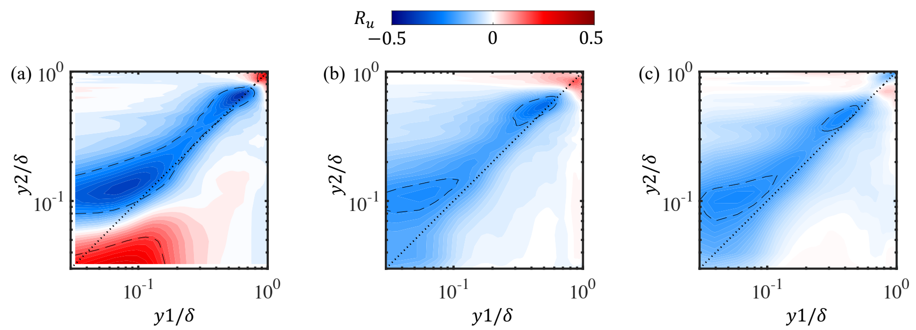

Figure 6. Amplitude modulation coefficients of streamwise velocity fluctuations $R_u(y1, y2)$ for the smooth and porous wall cases: (a) smooth wall; (b) small hole; (c) big hole. Black contour line: $|R_u| = 0.2$.

5 CONCLUSION

In the present study, the amplitude modulation effect of large-scale motions on small-scale fluctuations in a turbulent boundary layer over anisotropic porous walls is experimentally investigated using time-resolved particle image velocimetry. Two types of porous walls with different wall-normal permeabilities were applied by adjusting the diameter and distribution of the pores. The smooth wall condition was also tested for comparison. An overall skin reduction of more than 20% is achieved over both porous wall conditions.

The porous wall contributes to a notable disruption of positive large-scale structures when $y/\delta < 0.3$ due to the upwash and downwash motions, leading to the suppression of VISA events close to the wall. For the smooth wall case, the VISA events are caused by collisions between ejection and sweep motions which are possibly induced by a quasi-streamwise vortex. On the contrary, the VISA events in the near-wall region of the porous wall case are mainly caused by a low-speed fluid ejected away from the pore. The modulation of the multi-scale turbulent structures disrupts the near-wall cycle of turbulence, leading to the skin friction effect.

The analysis of the amplitude modulation phenomenon over the anisotropic porous wall indicates a remarkable attenuation of inner-outer interactions. The trend of spatial correlation between positive and negative large-scale structures with small-scale turbulence reverses compared with the smooth wall case. For the smooth wall case, the turbulent kinetic energy of the near-wall small-scale is excited by the pLSMs and suppressed by nLSMs. The opposite trend presents in the logarithmic region. However, for the anisotropic porous wall cases, the near-wall positive peak of the amplitude modulation coefficient not only disappears but even holds a negative value close to zero, indicating an inverse amplitude modulation effect. In the logarithmic region, the amplitude modulation effect is the same as that of the smooth wall case. Consequently, the small-scale turbulence is excited by the nLSMs in both near-wall and logarithmic regions.

ACKNOWLEDGEMENTS

This research has been supported by the National Key R&D Program of China (Grant No: 2020YFA0405700), National Natural Science Foundation of China (Grant No: 12372280, 92152109).

REFERENCES

W. P. Breugem, B. J. Boersma, and R. E. Uittenbogaard. The influence of wall permeability on turbulent channel flow. *Journal of Fluid Mechanics*, 562:35, 2006. doi: 10.1017/S0022112006000887.

Y. Kuwata and K. Suga. Direct numerical simulation of turbulence over anisotropic porous media. *Journal of Fluid Mechanics*, 831:41–71, 2017. doi: 10.1017/jfm.2017.619.

Garazi Gómez-de Segura and Ricardo García-Mayoral. Turbulent drag reduction by anisotropic permeable substrates–analysis and direct numerical simulations. *Journal of Fluid Mechanics*, 875:124–172, 2019.

Zhixiang Feng and Qingqing Ye. Turbulent boundary layer over porous media with wall-normal permeability. *Phyisics of Fluids*, 35(9):095111, 2023.

Nicholas Hutchins and Ivan Marusic. Large-scale influences in near-wall turbulence. *Philosophical Transactions of the Royal Society A: Mathematical, Physical and Engineering Sciences*, 365(1852):647–664, 2007. doi: 10.1098/rsta.2006.1942.

Christoph Efstathiou and Mitul Luhar. Mean turbulence statistics in boundary layers over high-porosity foams. *Journal of Fluid Mechanics*, 841:351–379, 2018. doi: 10.1017/jfm.2018.57.

Taehoon Kim, Gianluca Blois, James L. Best, and Kenneth T. Christensen. Experimental evidence of amplitude modulation in permeable-wall turbulence. *Journal of Fluid Mechanics*, 887:A3, 2020. doi: 10.1017/jfm.2019.1027.

A. J. Musker. Explicit expression for the smooth wall velocity distribution in a turbulent boundary layer. *AIAA Journal*, 17 (6):655–657, 1979. doi: 10.2514/3.61193.

Anthony Kendall and Manoochehr Koochesfahani. A method for estimating wall friction in turbulent wall-bounded flows. *Experiments in Fluids*, 44(5):773–780, 2008. doi: 10.1007/s00348-007-0433-9.

A. E. Perry and J. D. Li. Experimental support for the attached-eddy hypothesis in zero-pressure-gradient turbulent boundary layers. *Journal of Fluid Mechanics*, 218(-1):405, 1990. doi: 10.1017/S0022112090001057.

Ricardo Mejia-Alvarez. *Experimental study of low-order models of highly-irregular roughness and their impact on turbulent boundary layers*. PhD thesis, Univ. of Illinois at Urbana–Champaign, Urbana, IL, 2010.

Bharathram Ganapathisubramani, Ellen K. Longmire, and Ivan Marusic. Characteristics of vortex packets in turbulent boundary layers. *Journal of Fluid Mechanics*, 478(478): 35–46, 2003. doi: 10.1017/S0022112002003270.

C. Manes, D. Poggi, and L. Ridolfi. Turbulent boundary layers over permeable walls: Scaling and near-wall structure. *Journal of Fluid Mechanics*, 687:141–170, 2011. doi: 10.1017/jfm.2011.329.

R. F. Blackwelder and R. E. Kaplan. On the wall structure of the turbulent boundary layer. *Journal of Fluid Mechanics*, 76(1):89–112, 1976.

James M Wallace, Helmut Eckelmann, and Robert S Brodkey. The wall region in turbulent shear flow. *Journal of Fluid Mechanics*, 54(1):39–48, 1972.

K. Suga, M. Mori, and M. Kaneda. Vortex structure of turbulence over permeable walls. *International Journal of Heat and Fluid Flow*, 32(3):586–595, 2011. doi: 10.1016/j.ijheatfluidflow.2011.02.016.

Xiaonan Chen, Koji Iwano, Yasuhiko Sakai, and Yasumasa Ito. Effect of large-scale structures on bursting phenomenon in turbulent boundary layer. *International Journal of Heat and Fluid Flow*, 89:108811, 2021. doi: 10/gjqrd8.

D. Chung and B. J. McKEON. Large-eddy simulation of large-scale structures in long channel flow. *Journal of Fluid Mechanics*, 661:341–364, 2010. doi: 10.1017/S0022112010002995.

N. Hutchins, J. P. Monty, B. Ganapathisubramani, H. C.H. Ng, and I. Marusic. Three-dimensional conditional structure of a high-Reynolds-number turbulent boundary layer. *Journal of Fluid Mechanics*, 673:255–285, 2011. doi: 10.1017/S0022112010006245.

Gokul Pathikonda and Kenneth T. Christensen. Investigation of inner-outer interactions in a turbulent boundary layer using high-speed particle image velocimetry. *Physical Review Fluids*, 4(3):034607, 2019. doi: 10/gkgdw9.

Romain Mathis, Nicholas Hutchins, and Ivan Marusic. Large-scale amplitude modulation of the small-scale structures in turbulent boundary layers. *Journal of Fluid Mechanics*, 628:311–337, 2009. doi: 10.1017/S0022112009006946.

Hongyou Liu, Guohua Wang, and Xiaojing Zheng. Amplitude modulation between multi-scale turbulent motions in high-Reynolds-number atmospheric surface layers. *Journal of Fluid Mechanics*, 861:585–607, 2019. doi: 10/gn2v78.

Jinyul Hwang, Jin Lee, Hyung Jin Sung, and Tamer A Zaki. Inner-outer interactions of large-scale structures in turbulent channel flow. *Journal of Fluid Mechanics*, 790:128–157, 2016. doi: 10.1017/jfm.2016.3.

Sicong Wu, Kenneth T Christensen, and Carlos Pantano. Modelling smooth- and transitionally rough-wall turbulent channel flow by leveraging inner–outer interactions and principal component analysis. *Journal of Fluid Mechanics*, 863: 407–453, 2019.

Matteo Bernardini and Sergio Pirozzoli. Inner/outer layer interactions in turbulent boundary layers: A refined measure for the large-scale amplitude modulation mechanism. *Physics of Fluids*, 23(6):061701, 2011. doi: 10.1063/1.3589345.

Ronald J Adrian. Hairpin vortex organization in wall turbulence. *Physics of Fluids*, 19(4):41301, 2007. doi: 10.1063/1.2717527.

G. E. Elsinga, R. J. Adrian, B. W. Van Oudheusden, and F. Scarano. Three-dimensional vortex organization in a high-Reynolds-number supersonic turbulent boundary layer. *Journal of Fluid Mechanics*, 644:35–60, 2010. doi: 10.1017/S0022112009992047.

David J C Dennis and Timothy B. Nickels. Experimental measurement of large-scale three-dimensional structures in a turbulent boundary layer. part 1. vortex packets. *Journal of Fluid Mechanics*, 673:180–217, 2011. doi: 10.1017/S0022112010006324.